Editors' Suggestion | Featured in Physics

Magic-Angle Twisted Bilayer Graphene as a Topological Heavy Fermion Problem

Zhi-Da Song[1,2,*] and B. Andrei Bernevig[2,3,4]

[1]International Center for Quantum Materials, School of Physics, Peking University, Beijing 100871, China
[2]Department of Physics, Princeton University, Princeton, New Jersey 08544, USA
[3]Donostia International Physics Center, P. Manuel de Lardizabal 4, 20018 Donostia-San Sebastian, Spain
[4]IKERBASQUE, Basque Foundation for Science, 48009 Bilbao, Spain

(Received 29 November 2021; revised 4 May 2022; accepted 13 June 2022; published 19 July 2022)

Magic-angle ($\theta = 1.05°$) twisted bilayer graphene (MATBG) has shown two seemingly contradictory characters: the localization and quantum-dot-like behavior in STM experiments, and delocalization in transport experiments. We construct a model, which naturally captures the two aspects, from the Bistritzer-MacDonald (BM) model in a first principle spirit. A set of local flat-band orbitals (f) centered at the AA-stacking regions are responsible to the localization. A set of extended *topological* semimetallic conduction bands (c), which are at small energetic separation from the local orbitals, are responsible to the delocalization and transport. The topological flat bands of the BM model appear as a result of the hybridization of f and c electrons. This model then provides a new perspective for the strong correlation physics, which is now described as strongly correlated f electrons coupled to nearly free c electrons—we hence name our model as the topological heavy fermion model. Using this model, we obtain the U(4) and U(4) × U(4) symmetries of Refs. [1–5] as well as the correlated insulator phases and their energies. Simple rules for the ground states and their Chern numbers are derived. Moreover, features such as the large dispersion of the charge ±1 excitations [2,6,7], and the minima of the charge gap at the Γ_M point can now, for the first time, be understood both qualitatively and quantitatively in a simple physical picture. Our mapping opens the prospect of using heavy-fermion physics machinery to the superconducting physics of MATBG.

DOI: 10.1103/PhysRevLett.129.047601

Introduction.—Since the initial experimental discovery of the correlated insulator phases [8] and superconductivity [9] in, agic-angle ($\theta = 1.05°$) twisted bilayer graphene (MATBG) [10], extensive experimental [11–35] and theoretical [1–7,36–113] efforts have been made to understand the nature of these exotic phases. Theoretical challenges for understanding the correlation physics come from both the strong interaction compared to relatively small bandwidth as well as from the topology [36,38,41–43,104], which forbids a symmetric lattice description of the problem. The two flat bands of MATBG possess strong topology in the presence of $C_{2z}T$ (time-reversal followed by C_{2z} rotation) and particle-hole (P) symmetries [104], which supersedes the earlier, $C_{2z}T$ symmetry-protected fragile topology [41,42]. This strong topology extends to the entire continuum Bistritzer-MacDonald (BM) model, and implies the absence of a lattice model for any number of bands. The topology is also responsible to exotic phases such as quantum anomalous Hall states [2,5,55,60,82,84] and fractional Chern states [96,98,99,109].

Two types of complementary strategies have been proposed to resolve the problem of the lattice description. One is to construct extended Hubbard models [1,7,37,40,42,49,51,67,71], where either $C_{2z}T$ [1,7,40,49,67] or P [42] becomes nonlocal in real space. The other is to adopt a full momentum-space formalism [2,5,6,85,86,105,106,111], where locality becomes hidden. (Besides the two strategies, some phenomenological models are also proposed [39,48,63,64,90,92,97,100].) The real and momentum space strong coupling models elucidated the nature of the correlated insulator states: they are ferromagnets—sometimes carrying Chern numbers—in a large U(4) or U(4) × U(4) symmetry space that contains spin, valley, and band quantum number [1,2,4]. The dispersion of the excitations above the correlated insulators [2,6,7]—where superconductivity appears upon doping—is, despite being exact—not physically understood.

In the current Letter, nevertheless, we find it possible to write down a fully symmetric model that has a simple real space picture, which, remarkably and elegantly, solves the aforementioned puzzles. We reformulate and map the interacting MATBG as an effective topological heavy fermion system, which consists of local orbitals (f) centered at the AA-stacking regions and delocalized topological conduction bands (c). The f electrons are so localized that they have an almost zero kinetic energy (∼0.1 meV) but a strong on-site Coulomb repulsion that we compute to be ∼60 meV. The c electrons carry the symmetry anomaly and have unbounded kinetic energies. The actual flat bands of the BM model are from a

hybridization (∼20 meV) between the f and c bands. The interacting Hamiltonian also couples the f and c electrons through the presence of several types of interactions. Using this model, the ground states [1,2,44,50,53,65,68,71,77,84–86,114] and their topologies can be understood in a simple, physical picture. The quasiparticle excitation bandwidth can even be analytically determined.

Topological heavy fermion model.—The single-valley BM model has the symmetry of the magnetic space group $P6'2'2$, generated by C_{3z}, C_{2x}, $C_{2z}T$, and moiré translations. (See Refs. [41,115] for this group and its irreducible representations—irreps.) The energy bands in the valley $\eta = +$ of the BM model are shown in Fig. 1(b), where the bands are labeled by their irreps. References [41,42] showed that the irreps formed by the two flat bands, i.e., $\Gamma_1 \oplus \Gamma_2$; $M_1 \oplus M_2$; K_2K_3, are not consistent with any local orbitals (band representations [126]) and indicate a fragile [127–130] topological obstruction to a two-band lattice model. Here, we resolve the fragile topology by involving higher energy bands. Suppose we can "borrow" a Γ_3 irrep from higher (∼20 meV) energy bands and use it to replace the $\Gamma_1 \oplus \Gamma_2$ states; then the replaced irreps—Γ_3, $M_1 \oplus M_2$, and K_2K_3—are consistent with $p_x \pm ip_y$ orbitals located at the triangular lattice. We hence introduce two trial Gaussian-type Wannier functions (WFs) that transform as $p_x \pm ip_y$ orbitals under the crystalline symmetries. As indicated by the overlaps between the trial WFs and the Bloch bands [Fig. 1(a)], the trial WFs are supported by the flat band states at $\mathbf{k}$ away from Γ_M and by the lowest higher energy band states around Γ_M. Feeding the overlaps into the program WANNIER90 [116–118], we obtain the corresponding maximally localized WFs, density profile of which is shown in Fig. 1(b) [115]. (Similar local states are also discussed using different methods in Refs. [38,112].) These WFs are extremely localized—their nearest neighbor hoppings are about 0.1 meV—and span 96% percent of the flat bands.

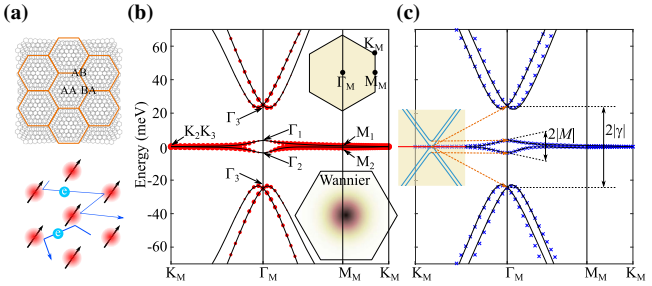

FIG. 1. Topological heavy fermion model. (a) A sketch of the moiré unit cell of MATBG and its heavy fermion analog, where the local moments and itinerant electrons are formed by the effective f orbitals at the AA-stacking regions and topological conduction bands (c), respectively. (b) The band structure of the BM model at the magic angle $\theta = 1.05°$, where the moiré BZ and high symmetry momenta are illustrated in the upper inset panel. The overlaps between the Bloch states and the trial WFs are represented by the red circles. The density profile of the constructed maximally localized WFs (f orbitals) is shown in the lower inset panel. (c) Bands given by the topological heavy fermion model (black lines) compared to the BM bands (blue crosses). The c (blue) and f bands (red) in the decoupled limit, where $\gamma = v'_\star = 0$, are shown in the inset. Orange dashed lines indicate the evolution of energy levels as f-c coupling is turned on.

To recover the irreps and topology of the middle two bands, we have to take into account the remaining 4% states, without which the localized electrons could not form a superconductor. To do this, we define the projector into the WFs as $\mathbb{P}$, the projector into the lowest six bands (per spin valley) as $\mathbb{I}$, and divide the low energy BM Hamiltonian H_{BM} into four parts: $H^{(f)} = \mathbb{P}H_{\mathrm{BM}}\mathbb{P}$, $H^{(c)} = \mathbb{Q}H_{\mathrm{BM}}\mathbb{Q}$, $H^{(fc)} = \mathbb{P}H_{\mathrm{BM}}\mathbb{Q}$, and $H^{(cf)} = H^{(fc)\dagger}$, where $\mathbb{Q} = \mathbb{I} - \mathbb{P}$, $H^{(c)}$ is the remaining Hamiltonian, and $H^{(fc)} + \mathrm{H.c.}$ is the coupling between WFs and the remaining states. As the couplings between WFs are extremely weak (∼0.1 meV) we find $H^{(f)} \approx 0$. Since the two states in $\mathbb{P}$ form Γ_3 at Γ_M, the four states in $\mathbb{Q}$ must form $\Gamma_3 \oplus \Gamma_1 \oplus \Gamma_2$ at Γ_M due to the irrep counting. Because of the crystalline and P symmetries, $H^{(c)}$ in the valley η takes the form [115]

$$H^{(c,\eta)}(\mathbf{k}) = \begin{pmatrix} 0_{2\times 2} & v_\star(\eta k_x\sigma_0 + ik_y\sigma_z) \\ v_\star(\eta k_x\sigma_0 - ik_y\sigma_z) & M\sigma_x \end{pmatrix} \tag{1}$$

to linear order of $\mathbf{k}$, where the first two-by-two block is spanned by the Γ_3 states and the second two-by-two block is spanned by the $\Gamma_1 \oplus \Gamma_2$ states. The Γ_1 and Γ_2 states are split by the M term [blue bands in Fig. 1(c)], while the Γ_3 states form a quadratic touching at $\mathbf{k} = 0$, which is shown in Ref. [115] responsible to the symmetry anomaly [104] jointly protected by $C_{2z}T$ and P. The coupling $H^{(fc)}$ in the valley η has the form

$$H^{(fc,\eta)}(\mathbf{k}) = [\gamma\sigma_0 + v'_\star(\eta k_x\sigma_x + k_y\sigma_y), 0_{2\times 2}], \tag{2}$$

where the second block is computed to be extremely small and hence is omitted and written as $0_{2\times 2}$. $H^{(fc,\eta)}$ will gap $H^{(c,\eta)}$, and hence provides for both the single particle gap and for the flat band topology of the BM model. Using a set of usually adopt parameters for MATBG, we find $v_\star = -4.303$ eV Å, $M = 3.697$ meV, $\gamma = -24.75$ meV, and $v'_\star = 1.622$ eV Å.

Since the WFs and the remaining "c" degrees of freedom have localized and plane-wave-like wave functions, respectively, we make the analogy with local orbitals and conduction bands in heavy fermion systems. We refer to them as local f orbitals and (topological) conduction c

bands, respectively. We use $f_{\mathbf{R}\alpha\eta s}$ ($\alpha = 1, 2$, $\eta = \pm$, $s = \uparrow, \downarrow$) to represent the annihilation operator of the αth WF of the valley η and spin s at the moiré unit cell $\mathbf{R}$. We use $c_{\mathbf{k}a\eta s}$ ($a = 1, 2, 3, 4$) to represent the annihilation operator of the ath conduction band basis of the valley η and spin s at the moiré momentum $\mathbf{k}$. The single-particle Hamiltonian can be written as

$$\hat{H}_0 = \sum_{|\mathbf{k}|<\Lambda_c}\sum_{aa'\eta s} H^{(c,\eta)}_{aa'}(\mathbf{k}) c^\dagger_{\mathbf{k}a\eta s} c_{\mathbf{k}a'\eta s} + \frac{1}{\sqrt{N}}\sum_{\substack{|\mathbf{k}|<\Lambda_c \\ \mathbf{R}}}\sum_{\alpha a\eta s}[e^{i\mathbf{k}\cdot\mathbf{R}-\frac{|\mathbf{k}|^2\lambda^2}{2}} H^{(fc,\eta)}_{\alpha a}(\mathbf{k}) f^\dagger_{\mathbf{R}\alpha\eta s} c_{\mathbf{k}a\eta s} + \text{H.c.}], \tag{3}$$

where Λ_c is the momentum cutoff for the c electrons, a_M is the moiré lattice constant, N is the number of moiré unit cell in the system, and λ, which is found to be $0.3375 a_M$, is a damping factor proportional to the size of WFs. We plot the band structure of $\hat{H}_0$ in Fig. 1(c), where the splitting of the two Γ_3 states is given by $2|\gamma|$ and the bandwidth of the two flat bands is given by $2M \approx 7.4$ meV. The spectrum of $\hat{H}_0$ matches very well with the BM model [Fig. 1(a)] in the energy range [−70 meV, 70 meV].

The U(4) symmetry.—The projected model of MATBG [1,2,4] is found to possess a U(4) symmetry if the kinetic energy of the flat bands is omitted. In the heavy fermion basis, this U(4) symmetry can be realized by imposing the flat band condition, i.e., $M = 0$. (Note that $2|M|$ is the bandwidth of the flat bands.) The U(4) moments of the f electrons, Γ_3 c electrons, and $\Gamma_1 \oplus \Gamma_2$ c electrons are given by [115]

$$\begin{aligned}
\hat{\Sigma}^{(f,\xi)}_{\mu\nu}(\mathbf{R}) &= \frac{\delta_{\xi,(-1)^{a-1}\eta}}{2} A^{\mu\nu}_{\alpha\eta s,\alpha'\eta' s'} f^\dagger_{\mathbf{R}\alpha\eta s} f_{\mathbf{R}\alpha'\eta' s'}, \\
\hat{\Sigma}^{(c\prime,\xi)}_{\mu\nu}(\mathbf{q}) &= \frac{\delta_{\xi,(-1)^{a-1}\eta}}{2N} A^{\mu\nu}_{a\eta s,a'\eta' s'} c^\dagger_{\mathbf{k}+\mathbf{q}a\eta s} c_{\mathbf{k}a'\eta' s'}, \quad (a = 1,2), \\
\hat{\Sigma}^{(c\prime\prime,\xi)}_{\mu\nu}(\mathbf{q}) &= \frac{\delta_{\xi,(-1)^{a-1}\eta}}{2N} B^{\mu\nu}_{a\eta s,a'\eta' s'} c^\dagger_{\mathbf{k}+\mathbf{q}a\eta s} c_{\mathbf{k}a'\eta' s'}, \quad (a = 3,4),
\end{aligned} \tag{4}$$

respectively, where repeated indices should be summed over and $A^{\mu\nu}$, $B^{\mu\nu}$ ($\mu, \nu = 0, x, y, z$) are eight-by-eight matrices

$$\begin{aligned}
A^{\mu\nu} &= \{\sigma_0\tau_0\varsigma_\nu, \sigma_y\tau_x\varsigma_\nu, \sigma_y\tau_y\varsigma_\nu, \sigma_0\tau_z\varsigma_\nu\}, \\
B^{\mu\nu} &= \{\sigma_0\tau_0\varsigma_\nu, -\sigma_y\tau_x\varsigma_\nu, -\sigma_y\tau_y\varsigma_\nu, \sigma_0\tau_z\varsigma_\nu\},
\end{aligned} \tag{5}$$

with $\sigma_{0,x,y,z}$, $\tau_{0,x,y,z}$, and $\varsigma_{0,x,y,z}$ being the Pauli or identity matrices for the orbital, valley, and spin degrees of freedom, respectively. The ±1 valued index ξ, equal to $(-1)^{\alpha-1}\eta$ or $(-1)^{a-1}\eta$ in the moments, labels different fundamental representations of the U(4) group. The global U(4) rotations are generated by $\hat{\Sigma}_{\mu\nu} = \sum_{\xi=\pm1} \hat{\Sigma}^{(f,\xi)}_{\mu\nu} + \hat{\Sigma}^{(c\prime,\xi)}_{\mu\nu} + \hat{\Sigma}^{(c\prime\prime,\xi)}_{\mu\nu}$. Unlike the U(4) rotations found in Refs. [1,2,4], which only commute the projected Hamiltonian into the flat bands, the U(4) rotations here commute with the full Hamiltonian. [Generators of the U(4) or U(4) × U(4) symmetry in the first chiral limit [36,102] is also given in Ref. [115].]

Interaction Hamiltonian.—To obtain the interaction Hamiltonian in the heavy fermion basis, we can first express the density operator $\rho(\mathbf{r})$ of the BM model in terms of $f_{\mathbf{R}\alpha\eta s}$ and $c_{\mathbf{k}a\eta s}$, and then substitute it into the Coulomb interaction, $\rho(\mathbf{r})V(\mathbf{r}-\mathbf{r}')\rho(\mathbf{r}')$. By evaluating the Coulomb integrals, we obtain the interaction Hamiltonian resembling a periodic Anderson model with extra f-c exchange interactions [115],

$$\hat{H}_I = \hat{H}_{U_1} + \hat{H}_J + \hat{H}_{U_2} + \hat{H}_V + \hat{H}_W. \tag{6}$$

$\hat{H}_{U_1} = (U_1/2)\sum_{\mathbf{R}} :\rho^f_{\mathbf{R}}::\rho^f_{\mathbf{R}}:$ are the on-site interactions of f electrons, where $\rho^f_{\mathbf{R}} = \sum_{\alpha\eta s} f^\dagger_{\mathbf{R}\alpha\eta s} f_{\mathbf{R}\alpha\eta s}$ is the f electrons density and the colon symbols represent the normal ordered operator with respect to the normal state.

$$\hat{H}_J = -J\sum_{\mathbf{Rq}}\sum_{\mu\nu}\sum_{\xi=\pm} e^{-i\mathbf{q}\cdot\mathbf{R}} :\hat{\Sigma}^{(f,\xi)}_{\mu\nu}(\mathbf{R})::\hat{\Sigma}^{(c\prime\prime,\xi)}_{\mu\nu}(\mathbf{q}): \tag{7}$$

is a ferromagnetic exchange coupling between U(4) moments of f electrons and $\Gamma_1 \oplus \Gamma_2$ c electrons. Using practical parameters for MATBG, we obtain $U_1 =$ 57.95 meV and $J = 16.38$ meV. The other three terms in $\hat{H}_I$ are the following: H_{U_2}, repulsion (∼2.3 meV) between nearest neighbor f electrons; H_V, repulsion (∼48 meV) between c electrons; and H_W, repulsion (∼47 meV) between c and f electrons.

As a widely adopted approximation in heavy fermion materials, $\hat{H}_{U_2} + \hat{H}_V + \hat{H}_W$ can be decoupled in the Hartree channel due to the delocalized and localized natures of c and f electrons. Hence, these terms only effectively shift the band energies of f and c bands. Then, U_1—the on-site repulsion of the f electrons—is by far the largest energy scale of the problem—more than twice the hybridization (γ) and three times the exchange (J). In Hartree-Fock (HF) calculations U_1 is found to be the source of spontaneous symmetry breakings.

Ground states.—Since U_1 is much larger than the couplings [γ, J, $v'_\star(\eta k_x\sigma_x + k_y\sigma_y)$] between f and c electrons, a reasonable guess of the ground states would be product states of f multiplets and the (gapless point) Fermi liquid state ($|F\rangle$) of the half-filled c electrons. We call such product states "the parent states." E.g., the parent valley-polarized (V) state at the charge neutrality ($\nu = 0$) is

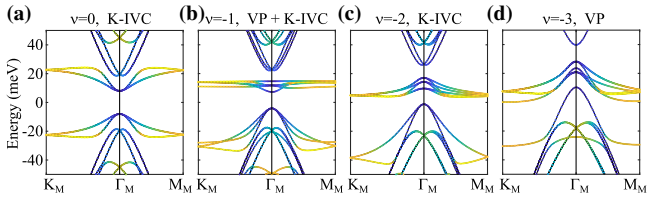

FIG. 2. The self-consistent HF bands upon the ground states at the fillings $\nu = 0, -1, -2, -3$. The color of the bands represent the contributing components, wherein yellow represents the f-electron states and blue represents the c-electron states.

$$|V_0^{\nu=0}\rangle = \prod_{\mathbf{R}} \prod_{\alpha=1,2} \prod_{s=\uparrow\downarrow} f^\dagger_{\mathbf{R},\alpha,+,s}|F\rangle. \tag{8}$$

The parent Kramers intervalley-coherent (K) state is a U(4)-rotation of $|V_0^{\nu=0}\rangle$ along the τ_x direction

$$\begin{aligned}|K_0^{\nu=0}\rangle &= e^{-i\frac{\pi}{2}\hat{\Sigma}_{x0}}|V_0^{\nu=0}\rangle \\ &= \prod_{\mathbf{R}} \prod_{s=\uparrow\downarrow} \frac{1}{2}(f^\dagger_{\mathbf{R},1,+,s} + f^\dagger_{\mathbf{R},2,-,s}) \\ &\times (-f^\dagger_{\mathbf{R},1,-,s} + f^\dagger_{\mathbf{R},2,+,s})|F\rangle. \end{aligned} \tag{9}$$

Parent states at other integer fillings ($\nu = 0, \pm1, \pm2, \pm3$) can be similarly constructed [115]. They would be ground states of the Hamiltonian if γ, J, $v'_\star$ terms vanished; hybridization of f and c electrons will develop, i.e., $\langle f^\dagger c\rangle \neq 0$, otherwise. The determination of ground states by self-consistent HF calculation with initial states given by the parent states is given in Ref. [115]. The numerically found HF ground states at the integer fillings (Fig. 2) are fully consistent with those in Ref. [5].

The parent states are such good initial states for the HF calculations that the one-shot HF is already qualitatively the same as the self-consistent HF (see Fig. 3). Thanks to the simplicity of the heavy fermion model, the one-shot energies can be analytically estimated and we are able to derive two rules for the ground states [115]. *First*, in the parent state, f electrons at each site tend to be symmetric under permutation of U(4) indices to save the Coulomb energy (Hund's rule). Both Eqs. (8) and (9) satisfy the first rule. *Second*, for U(4)-related states at a given integer filling ν, the state that minimizes $\hat{H}_M + \hat{H}_J$ is the ground state, where $\hat{H}_M$ is the U(4)-breaking M term in $\hat{H}_0$ [Eq. (1)]. This energy can be estimated by the lowest $\nu + 4$ levels of the mean field Hamiltonian $H^{(\Gamma_1\oplus\Gamma_2)}$ spanned by the $\Gamma_1 \oplus \Gamma_2$ basis of the c bands at $\mathbf{k} = 0$, which reads (up to constants)

$$H^{(\Gamma_1\oplus\Gamma_2)} = M\sigma_x\tau_0\varsigma_0 - \frac{J}{2}(\tau_z\bar{O}^{fT}\tau_z + \sigma_z\bar{O}^{fT}\sigma_z). \tag{10}$$

Here, $\bar{O}^f_{\alpha\eta s,\alpha'\eta' s'} = \langle f^\dagger_{\mathbf{R}\alpha\eta s} f_{\mathbf{R}\alpha'\eta' s'}\rangle - \frac{1}{2}\delta_{\alpha\alpha'}\delta_{\eta\eta'}\delta_{ss'}$ is the density matrix of the local f orbitals with homogeneity assumed.

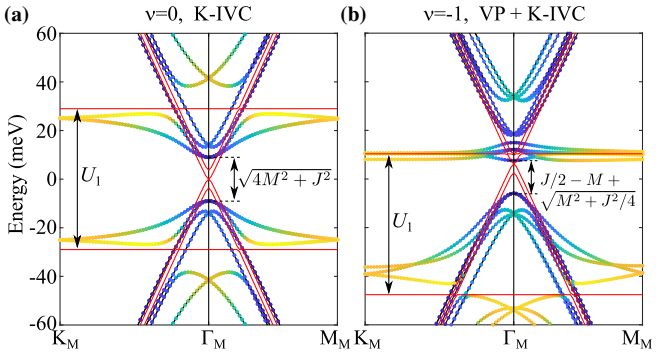

FIG. 3. The one-shot HF bands of the ground states at the fillings $\nu = 0, -1$. The red solid bands are the quasiparticle bands of the decoupled Hamiltonian, where $\gamma = v'_\star = J = 0$. The horizontal and dispersive red bands are of the f and c electrons, respectively. The touching point of the dispersive red bands at Γ_M is quadratic, while since M is small, it may look like linear. The one-shot bands can be understood as a result of hybridization between f and c electrons.

We have assumed that, for all the integer fillings, the eight lowest energy levels (closest to the gap) are always contributed by the $\Gamma_1 \oplus \Gamma_2$ c-band basis—which are part of the flat bands—hence we only need to look at the $\Gamma_1 \oplus \Gamma_2$ subspace. This assumption is fully justified by previous studies based on two-band projected Hamiltonian, where only $\Gamma_1 \oplus \Gamma_2$ basis exists, and will become clearer after we discuss the charge ±1 excitations.

We now apply the second rule to Eqs. (8) and (9) to determine the one-shot state of lowest energy. $\bar{O}^f$ matrices given by Eqs. (8) and (9) are $\frac{1}{2}\sigma_0\tau_z\varsigma_0$ and $-\frac{1}{2}\sigma_y\tau_y\varsigma_0$, respectively; the resulted lowest four levels of $H^{(\Gamma_1\oplus\Gamma_2)}$ are $\pm M - J/2$ (each twofold) and $-\sqrt{M^2 + J^2/4}$ (fourfold), respectively. It is direct to verify that the latter (K) has a lower energy. Applying the two rules to parent states at other fillings, we obtain consistent results with the full numerical calculations in Refs. [5,105]. We also obtain an analytical expression for the Chern numbers of ground states [115].

Charge ±1 *excitations.*—As shown in Figs. 2 and 3 HFbands-maintext,fig:excitation-maintext and in Refs. [2,6,7,85,86,110], at $\mathbf{k}$ away from Γ_M, the quasiparticle bands have a large gap ($\sim U_1$) and are relatively flat; at $\mathbf{k}$ around Γ_M, the bands have significant dip. Such features are found related to the topology of the two flat bands [6,7] but have not yet been quantitatively understood. The heavy fermion model provides a natural explanation to these features. We first consider the decoupled limit ($\gamma = v'_\star = J = 0$) at $\nu = 0$, where the f-electron bands are flat and have a (charge) gap U_1, and the c-electron bands are given by $H^{(c,\eta)}$ [Fig. 3(a)]. Tuning on γ, $v'_\star$, and J then yields the one-shot quasiparticle bands. At $\mathbf{k} = 0$, γ gaps out the Γ_3 c bands, and J further gaps out the $\Gamma_1 \oplus \Gamma_2$ c bands. As the splitting of $\Gamma_1 - \Gamma_2$ is smaller than that of

the Γ_3, the lowest excitations will carry Γ_1, Γ_2 representations, matching Refs. [2,6,7] and, according to the discussion after Eq. (10), equals to $2\sqrt{M^2+J^2/4}$ and $|J-2M|$ for K and V states, respectively. At $\mathbf{k}\neq 0$, the $v'_\star$ term hybridizes the flat f bands and dispersive c bands. For large $\mathbf{k}$, where the c bands have very high kinetic energies, the hybridization is relatively weak and the gap is still approximately U_1. Thus, the shape of the quasiparticle bands is explained, and its bandwidth is approximately given by $(U_1-J)/2$ when M is small. As discussed in Ref. [115], the feature that the larger ($\sim U_1$) and smaller ($\sim J$) gaps are contributed by f and c electrons, respectively, is reflected in the STM spectra and Landau levels at different regions (AA or AB sites) of MATBG.

At nonzero fillings, the quasiparticle bands can also be understood as hybridized flat f bands and dispersive c bands, except that the f and c bands may feel different effective chemical potentials due to the density-density interactions between them. For example, at $\nu=-1$, the upper branch of the f bands is shifted to an energy close to the quadratic touching of the c bands [Fig. 3(b)] [115]. Thus, one of the hybridized bands is extremely flat.

Discussion.—The coexistence of quantum-dot-like behavior [21,25] and superconductivity [9,11,12,14,15] may now be understood—they come from two different types (f and c) of carriers. In fact, inspired by the Pomeranchuk effect experiments [33,34] and strange metal behavior [19,20], authors of Refs. [33,34,107] also conjecture the possibility of coexistence of local momenta and itinerant electrons. (The heavy fermion theory analog may also exist in other twisted materials [131].) Our Letter *derives* and shows the exact mapping of MATBG to such a heavy-fermion type model. As such, the machinery of heavy fermions [132–146] can now be applied, for the first time, to MATBG. We speculate that it will lead to pairing [52,54,56–59,66,70,78–80,91,94,95,108] in nontrivial gap channels.

We thank X. Dai, O Vafek, A. Yazdani, P. Coleman, E.-A. Kim, Q. Si, R Fernandez, P. Jarillo-Herrero and D. Efetov for discussions. Z.-D. S. was supported by DOE Grant No. DE-SC0016239 and National Key Research and Development Program of China (No. 2021YFA1401900). B. A. B. was supported by DOE Grant No. DE-SC0016239. Additional support was provided by Gordon and Betty Moore Foundation through Grant No. GBMF8685 toward the Princeton theory program.

*songzd@pku.edu.cn

[1] Jian Kang and Oskar Vafek, Strong Coupling Phases of Partially Filled Twisted Bilayer Graphene Narrow Bands, Phys. Rev. Lett. **122**, 246401 (2019).

[2] Nick Bultinck, Eslam Khalaf, Shang Liu, Shubhayu Chatterjee, Ashvin Vishwanath, and Michael P. Zaletel, Ground State and Hidden Symmetry of Magic-Angle Graphene at Even Integer Filling, Phys. Rev. X **10**, 031034 (2020).

[3] Oskar Vafek and Jian Kang, Renormalization Group Study of Hidden Symmetry in Twisted Bilayer Graphene with Coulomb Interactions, Phys. Rev. Lett. **125**, 257602 (2020).

[4] B. Andrei Bernevig, Zhi-Da Song, Nicolas Regnault, and Biao Lian, Twisted bilayer graphene. III. Interacting Hamiltonian and exact symmetries, Phys. Rev. B **103**, 205413 (2021).

[5] Biao Lian, Zhi-Da Song, Nicolas Regnault, Dmitri K. Efetov, Ali Yazdani, and B. Andrei Bernevig, Twisted bilayer graphene. IV. Exact insulator ground states and phase diagram, Phys. Rev. B **103**, 205414 (2021).

[6] B. Andrei Bernevig, Biao Lian, Aditya Cowsik, Fang Xie, Nicolas Regnault, and Zhi-Da Song, Twisted bilayer graphene. V. Exact analytic many-body excitations in Coulomb Hamiltonians: Charge gap, Goldstone modes, and absence of Cooper pairing, Phys. Rev. B **103**, 205415 (2021).

[7] Oskar Vafek and Jian Kang, Lattice model for the Coulomb interacting chiral limit of the magic angle twisted bilayer graphene: Symmetries, obstructions and excitations, Phys. Rev. B **104**, 075143 (2021).

[8] Yuan Cao, Valla Fatemi, Ahmet Demir, Shiang Fang, Spencer L. Tomarken, Jason Y. Luo, Javier D. Sanchez-Yamagishi, Kenji Watanabe, Takashi Taniguchi, Efthimios Kaxiras, Ray C. Ashoori, and Pablo Jarillo-Herrero, Correlated insulator behaviour at half-filling in magic-angle graphene superlattices, Nature (London) **556**, 80 (2018).

[9] Yuan Cao, Valla Fatemi, Shiang Fang, Kenji Watanabe, Takashi Taniguchi, Efthimios Kaxiras, and Pablo Jarillo-Herrero, Unconventional superconductivity in magic-angle graphene superlattices, Nature (London) **556**, 43 (2018).

[10] Rafi Bistritzer and Allan H. MacDonald, Moiré bands in twisted double-layer graphene, Proc. Natl. Acad. Sci. U.S.A. **108**, 12233 (2011).

[11] Xiaobo Lu, Petr Stepanov, Wei Yang, Ming Xie, Mohammed Ali Aamir, Ipsita Das, Carles Urgell, Kenji Watanabe, Takashi Taniguchi, Guangyu Zhang, Adrian Bachtold, Allan H. MacDonald, and Dmitri K. Efetov, Superconductors, orbital magnets and correlated states in magic-angle bilayer graphene, Nature (London) **574**, 653 (2019).

[12] Matthew Yankowitz, Shaowen Chen, Hryhoriy Polshyn, Yuxuan Zhang, K Watanabe, T Taniguchi, David Graf, Andrea F Young, and Cory R Dean, Tuning superconductivity in twisted bilayer graphene, Science **363**, 1059 (2019).

[13] Aaron L. Sharpe, Eli J. Fox, Arthur W. Barnard, Joe Finney, Kenji Watanabe, Takashi Taniguchi, M. A. Kastner, and David Goldhaber-Gordon, Emergent ferromagnetism near three-quarters filling in twisted bilayer graphene, Science **365**, 605 (2019).

[14] Yu Saito, Jingyuan Ge, Kenji Watanabe, Takashi Taniguchi, and Andrea F. Young, Independent superconductors and correlated insulators in twisted bilayer graphene, Nat. Phys. **16**, 926 (2020).

[15] Petr Stepanov, Ipsita Das, Xiaobo Lu, Ali Fahimniya, Kenji Watanabe, Takashi Taniguchi, Frank H. L. Koppens, Johannes Lischner, Leonid Levitov, and Dmitri K. Efetov, Untying the insulating and superconducting orders in magic-angle graphene, Nature (London) **583**, 375 (2020).

[16] Xiaoxue Liu, Zhi Wang, Kenji Watanabe, Takashi Taniguchi, Oskar Vafek, and JIA Li, Tuning electron correlation in magic-angle twisted bilayer graphene using Coulomb screening, Science **371**, 1261 (2021).

[17] Harpreet Singh Arora, Robert Polski, Yiran Zhang, Alex Thomson, Youngjoon Choi, Hyunjin Kim, Zhong Lin, Ilham Zaky Wilson, Xiaodong Xu, Jiun-Haw Chu *et al.*, Superconductivity in metallic twisted bilayer graphene stabilized by We_2, Nature (London) **583**, 379 (2020).

[18] M. Serlin, C. L. Tschirhart, H. Polshyn, Y. Zhang, J. Zhu, K. Watanabe, T. Taniguchi, L. Balents, and A. F. Young, Intrinsic quantized anomalous Hall effect in a moiré heterostructure, Science **367**, 900 (2020).

[19] Yuan Cao, Debanjan Chowdhury, Daniel Rodan-Legrain, Oriol Rubies-Bigorda, Kenji Watanabe, Takashi Taniguchi, T. Senthil, and Pablo Jarillo-Herrero, Strange Metal in Magic-Angle Graphene with Near Planckian Dissipation, Phys. Rev. Lett. **124**, 076801 (2020).

[20] Hryhoriy Polshyn, Matthew Yankowitz, Shaowen Chen, Yuxuan Zhang, K. Watanabe, T. Taniguchi, Cory R. Dean, and Andrea F. Young, Large linear-in-temperature resistivity in twisted bilayer graphene, Nat. Phys. **15**, 1011 (2019).

[21] Yonglong Xie, Biao Lian, Berthold Jäck, Xiaomeng Liu, Cheng-Li Chiu, Kenji Watanabe, Takashi Taniguchi, B Andrei Bernevig, and Ali Yazdani, Spectroscopic signatures of many-body correlations in magic-angle twisted bilayer graphene, Nature (London) **572**, 101 (2019).

[22] Youngjoon Choi, Jeannette Kemmer, Yang Peng, Alex Thomson, Harpreet Arora, Robert Polski, Yiran Zhang, Hechen Ren, Jason Alicea, Gil Refael *et al.*, Electronic correlations in twisted bilayer graphene near the magic angle, Nat. Phys. **15**, 1174 (2019).

[23] Alexander Kerelsky, Leo J. McGilly, Dante M. Kennes, Lede Xian, Matthew Yankowitz, Shaowen Chen, K. Watanabe, T. Taniguchi, James Hone, Cory Dean *et al.*, Maximized electron interactions at the magic angle in twisted bilayer graphene, Nature (London) **572**, 95 (2019).

[24] Yuhang Jiang, Xinyuan Lai, Kenji Watanabe, Takashi Taniguchi, Kristjan Haule, Jinhai Mao, and Eva Y. Andrei, Charge order and broken rotational symmetry in magic-angle twisted bilayer graphene, Nature (London) **573**, 91 (2019).

[25] Dillon Wong, Kevin P. Nuckolls, Myungchul Oh, Biao Lian, Yonglong Xie, Sangjun Jeon, Kenji Watanabe, Takashi Taniguchi, B. Andrei Bernevig, and Ali Yazdani, Cascade of electronic transitions in magic-angle twisted bilayer graphene, Nature (London) **582**, 198 (2020).

[26] U. Zondiner, A. Rozen, D. Rodan-Legrain, Y. Cao, R. Queiroz, T. Taniguchi, K. Watanabe, Y. Oreg, F. von Oppen, Ady Stern *et al.*, Cascade of phase transitions and Dirac revivals in magic-angle graphene, Nature (London) **582**, 203 (2020).

[27] Kevin P Nuckolls, Myungchul Oh, Dillon Wong, Biao Lian, Kenji Watanabe, Takashi Taniguchi, B Andrei Bernevig, and Ali Yazdani, Strongly correlated Chern insulators in magic-angle twisted bilayer graphene, Nature (London) **588**, 610 (2020).

[28] Youngjoon Choi, Hyunjin Kim, Yang Peng, Alex Thomson, Cyprian Lewandowski, Robert Polski, Yiran Zhang, Harpreet Singh Arora, Kenji Watanabe, Takashi Taniguchi *et al.*, Correlation-driven topological phases in magic-angle twisted bilayer graphene, Nature (London) **589**, 536 (2021).

[29] Yu Saito, Jingyuan Ge, Louk Rademaker, Kenji Watanabe, Takashi Taniguchi, Dmitry A Abanin, and Andrea F. Young, Hofstadter subband ferromagnetism and symmetry-broken Chern insulators in twisted bilayer graphene, Nat. Phys. **17**, 478 (2021).

[30] Ipsita Das, Xiaobo Lu, Jonah Herzog-Arbeitman, Zhi-Da Song, Kenji Watanabe, Takashi Taniguchi, B. Andrei Bernevig, and Dmitri K. Efetov, Symmetry-broken Chern insulators and Rashba-like Landau-level crossings in magic-angle bilayer graphene, Nat. Phys. **17**, 710 (2021).

[31] Shuang Wu, Zhenyuan Zhang, K. Watanabe, T. Taniguchi, and Eva Y. Andrei, Chern insulators, van hove singularities and topological flat bands in magic-angle twisted bilayer graphene, Nat. Mater. **20**, 488 (2021).

[32] Jeong Min Park, Yuan Cao, Kenji Watanabe, Takashi Taniguchi, and Pablo Jarillo-Herrero, Flavour Hund's coupling, Chern gaps and charge diffusivity in moiré graphene, Nature (London) **592**, 43 (2021).

[33] Yu Saito, Fangyuan Yang, Jingyuan Ge, Xiaoxue Liu, Takashi Taniguchi, Kenji Watanabe, JIA Li, Erez Berg, and Andrea F. Young, Isospin Pomeranchuk effect in twisted bilayer graphene, Nature (London) **592**, 220 (2021).

[34] Asaf Rozen, Jeong Min Park, Uri Zondiner, Yuan Cao, Daniel Rodan-Legrain, Takashi Taniguchi, Kenji Watanabe, Yuval Oreg, Ady Stern, Erez Berg *et al.*, Entropic evidence for a Pomeranchuk effect in magic-angle graphene, Nature (London) **592**, 214 (2021).

[35] Xiaobo Lu, Biao Lian, Gaurav Chaudhary, Benjamin A. Piot, Giulio Romagnoli, Kenji Watanabe, Takashi Taniguchi, Martino Poggio, Allan H. MacDonald, B. Andrei Bernevig, and Dmitri K. Efetov, Multiple flat bands and topological Hofstadter butterfly in twisted bilayer graphene close to the second magic angle, Proc. Natl. Acad. Sci. U.S.A. **118**, e2100006118 (2021).

[36] Grigory Tarnopolsky, Alex Jura Kruchkov, and Ashvin Vishwanath, Origin of Magic Angles in Twisted Bilayer Graphene, Phys. Rev. Lett. **122**, 106405 (2019).

[37] Liujun Zou, Hoi Chun Po, Ashvin Vishwanath, and T. Senthil, Band structure of twisted bilayer graphene: Emergent symmetries, commensurate approximants, and Wannier obstructions, Phys. Rev. B **98**, 085435 (2018).

[38] Jianpeng Liu, Junwei Liu, and Xi Dai, Pseudo landau level representation of twisted bilayer graphene: Band topology and implications on the correlated insulating phase, Phys. Rev. B **99**, 155415 (2019).

[39] Dmitry K. Efimkin and Allan H. MacDonald, Helical network model for twisted bilayer graphene, Phys. Rev. B **98**, 035404 (2018).

[40] Jian Kang and Oskar Vafek, Symmetry, Maximally Localized Wannier States, and a Low-Energy Model for Twisted Bilayer Graphene Narrow Bands, Phys. Rev. X **8**, 031088 (2018).
[41] Zhida Song, Zhijun Wang, Wujun Shi, Gang Li, Chen Fang, and B. Andrei Bernevig, All Magic Angles in Twisted Bilayer Graphene are Topological, Phys. Rev. Lett. **123**, 036401 (2019).
[42] Hoi Chun Po, Liujun Zou, T. Senthil, and Ashvin Vishwanath, Faithful tight-binding models and fragile topology of magic-angle bilayer graphene, Phys. Rev. B **99**, 195455 (2019).
[43] Kasra Hejazi, Chunxiao Liu, Hassan Shapourian, Xiao Chen, and Leon Balents, Multiple topological transitions in twisted bilayer graphene near the first magic angle, Phys. Rev. B **99**, 035111 (2019).
[44] Bikash Padhi, Chandan Setty, and Philip W. Phillips, Doped twisted bilayer graphene near magic angles: Proximity to Wigner crystallization, not mott insulation, Nano Lett. **18**, 6175 (2018).
[45] Biao Lian, Fang Xie, and B. Andrei Bernevig, Landau level of fragile topology, Phys. Rev. B **102**, 041402(R) (2020).
[46] Kasra Hejazi, Chunxiao Liu, and Leon Balents, Landau levels in twisted bilayer graphene and semiclassical orbits, Phys. Rev. B **100**, 035115 (2019).
[47] Bikash Padhi, Apoorv Tiwari, Titus Neupert, and Shinsei Ryu, Transport across twist angle domains in moiré graphene, Phys. Rev. Research **2**, 033458 (2020).
[48] Cenke Xu and Leon Balents, Topological Superconductivity in Twisted Multilayer Graphene, Phys. Rev. Lett. **121**, 087001 (2018).
[49] Mikito Koshino, Noah F. Q. Yuan, Takashi Koretsune, Masayuki Ochi, Kazuhiko Kuroki, and Liang Fu, Maximally Localized Wannier Orbitals and the Extended Hubbard Model for Twisted Bilayer Graphene, Phys. Rev. X **8**, 031087 (2018).
[50] Masayuki Ochi, Mikito Koshino, and Kazuhiko Kuroki, Possible correlated insulating states in magic-angle twisted bilayer graphene under strongly competing interactions, Phys. Rev. B **98**, 081102(R) (2018).
[51] Xiao Yan Xu, K. T. Law, and Patrick A. Lee, Kekulé valence bond order in an extended Hubbard model on the honeycomb lattice with possible applications to twisted bilayer graphene, Phys. Rev. B **98**, 121406(R) (2018).
[52] Francisco Guinea and Niels R. Walet, Electrostatic effects, band distortions, and superconductivity in twisted graphene bilayers, Proc. Natl. Acad. Sci. U.S.A. **115**, 13174 (2018).
[53] Jörn W. F. Venderbos and Rafael M. Fernandes, Correlations and electronic order in a two-orbital honeycomb lattice model for twisted bilayer graphene, Phys. Rev. B **98**, 245103 (2018).
[54] Y.-Z. You and A. Vishwanath, Superconductivity from valley fluctuations and approximate SO(4) symmetry in a weak coupling theory of twisted bilayer graphene, npj Quantum Mater. **4**, 16 (2019).
[55] Fengcheng Wu and Sankar Das Sarma, Collective Excitations of Quantum Anomalous Hall Ferromagnets in Twisted Bilayer Graphene, Phys. Rev. Lett. **124**, 046403 (2020).
[56] Biao Lian, Zhijun Wang, and B. Andrei Bernevig, Twisted Bilayer Graphene: A PhononDriven Superconductor, Phys. Rev. Lett. **122**, 257002 (2019).
[57] Fengcheng Wu, A. H. MacDonald, and Ivar Martin, Theory of Phonon-Mediated Superconductivity in Twisted Bilayer Graphene, Phys. Rev. Lett. **121**, 257001 (2018).
[58] Hiroki Isobe, Noah F. Q. Yuan, and Liang Fu, Unconventional Superconductivity and Density Waves in Twisted Bilayer Graphene, Phys. Rev. X **8**, 041041 (2018).
[59] Cheng-Cheng Liu, Li-Da Zhang, Wei-Qiang Chen, and Fan Yang, Chiral Spin Density Wave and $d + id$ Superconductivity in the Magic-Angle-Twisted Bilayer Graphene, Phys. Rev. Lett. **121**, 217001 (2018).
[60] Nick Bultinck, Shubhayu Chatterjee, and Michael P. Zaletel, Mechanism for Anomalous Hall Ferromagnetism in Twisted Bilayer Graphene, Phys. Rev. Lett. **124**, 166601 (2020).
[61] Ya-Hui Zhang, Dan Mao, Yuan Cao, Pablo Jarillo-Herrero, and T Senthil, Nearly flat Chern bands in moiré superlattices, Phys. Rev. B **99**, 075127 (2019).
[62] Jianpeng Liu, Zhen Ma, Jinhua Gao, and Xi Dai, Quantum Valley Hall Effect, Orbital Magnetism, and Anomalous Hall Effect in Twisted Multilayer Graphene Systems, Phys. Rev. X **9**, 031021 (2019).
[63] Xiao-Chuan Wu, Chao-Ming Jian, and Cenke Xu, Coupled-wire description of the correlated physics in twisted bilayer graphene, Phys. Rev. B **99**, 161405 (2019).
[64] Alex Thomson, Shubhayu Chatterjee, Subir Sachdev, and Mathias S. Scheurer, Triangular antiferromagnetism on the honeycomb lattice of twisted bilayer graphene, Phys. Rev. B **98**, 075109 (2018).
[65] John F. Dodaro, Steven A. Kivelson, Yoni Schattner, Xiao-Qi Sun, and Chao Wang, Phases of a phenomenological model of twisted bilayer graphene, Phys. Rev. B **98**, 075154 (2018).
[66] Jose Gonzalez and Tobias Stauber, Kohn-Luttinger Superconductivity in Twisted Bilayer Graphene, Phys. Rev. Lett. **122**, 026801 (2019).
[67] Noah FQ Yuan and Liang Fu, Model for the metal-insulator transition in graphene superlattices and beyond, Phys. Rev. B **98**, 045103 (2018).
[68] Kangjun Seo, Valeri N. Kotov, and Bruno Uchoa, Ferromagnetic Mott State in Twisted Graphene Bilayers at the Magic Angle, Phys. Rev. Lett. **122**, 246402 (2019).
[69] Kasra Hejazi, Xiao Chen, and Leon Balents, Hybrid Wannier Chern bands in magic angle twisted bilayer graphene and the quantized anomalous Hall effect, Phys. Rev. Research **3**, 013242 (2021).
[70] Eslam Khalaf, Shubhayu Chatterjee, Nick Bultinck, Michael P Zaletel, and Ashvin Vishwanath, Charged skyrmions and topological origin of superconductivity in magic-angle graphene, Sci. Adv. **7**, eabf5299 (2021).
[71] Hoi Chun Po, Liujun Zou, Ashvin Vishwanath, and T. Senthil, Origin of Mott Insulating Behavior and Superconductivity in Twisted Bilayer Graphene, Phys. Rev. X **8**, 031089 (2018).

[72] Fang Xie, Zhida Song, Biao Lian, and B. Andrei Bernevig, Topology-Bounded Superfluid Weight in Twisted Bilayer Graphene, Phys. Rev. Lett. **124**, 167002 (2020).
[73] A. Julku, T. J. Peltonen, L. Liang, T. T. Heikkilä, and P. Törmä, Superfluid weight and Berezinskii-Kosterlitz-Thouless transition temperature of twisted bilayer graphene, Phys. Rev. B **101**, 060505(E) (2020).
[74] Xiang Hu, Timo Hyart, Dmitry I. Pikulin, and Enrico Rossi, Geometric and Conventional Contribution to the Superfluid Weight in Twisted Bilayer Graphene, Phys. Rev. Lett. **123**, 237002 (2019).
[75] Jian Kang and Oskar Vafek, Non-Abelian Dirac node braiding and near-degeneracy of correlated phases at odd integer filling in magic-angle twisted bilayer graphene, Phys. Rev. B **102**, 035161 (2020).
[76] Tomohiro Soejima, Daniel E. Parker, Nick Bultinck, Johannes Hauschild, and Michael P. Zaletel, Efficient simulation of moiré materials using the density matrix renormalization group, Phys. Rev. B **102**, 205111 (2020).
[77] Jed H. Pixley and Eva Y. Andrei, Ferromagnetism in magic-angle graphene, Science **365**, 543 (2019).
[78] E. J. König, Piers Coleman, and A. M. Tsvelik, Spin magnetometry as a probe of stripe superconductivity in twisted bilayer graphene, Phys. Rev. B **102**, 104514 (2020).
[79] Maine Christos, Subir Sachdev, and Mathias S. Scheurer, Superconductivity, correlated insulators, and Wess-Zumino-Witten terms in twisted bilayer graphene, Proc. Natl. Acad. Sci. U.S.A. **117**, 29543 (2020).
[80] Cyprian Lewandowski, Debanjan Chowdhury, and Jonathan Ruhman, Pairing in magic-angle twisted bilayer graphene: Role of phonon and plasmon umklapp, Phys. Rev. B **103**, 235401 (2021).
[81] Yves H. Kwan, S. A. Parameswaran, and S. L. Sondhi, Twisted bilayer graphene in a parallel magnetic field, Phys. Rev. B **101**, 205116 (2020).
[82] Yves H. Kwan, Yichen Hu, Steven H. Simon, and S. A. Parameswaran, Exciton Band Topology in Spontaneous Quantum Anomalous Hall Insulators: Applications to Twisted Bilayer Graphene, Phys. Rev. Lett. **126**, 137601 (2021).
[83] Ming Xie and A. H. MacDonald, Nature of the Correlated Insulator States in Twisted Bilayer Graphene, Phys. Rev. Lett. **124**, 097601 (2020).
[84] Jianpeng Liu and Xi Dai, Theories for the correlated insulating states and quantum anomalous Hall effect phenomena in twisted bilayer graphene, Phys. Rev. B **103**, 035427 (2021).
[85] Tommaso Cea and Francisco Guinea, Band structure and insulating states driven by Coulomb interaction in twisted bilayer graphene, Phys. Rev. B **102**, 045107 (2020).
[86] Yi Zhang, Kun Jiang, Ziqiang Wang, and Fuchun Zhang, Correlated insulating phases of twisted bilayer graphene at commensurate filling fractions: A Hartree-Fock study, Phys. Rev. B **102**, 035136 (2020).
[87] Shang Liu, Eslam Khalaf, Jong Yeon Lee, and Ashvin Vishwanath, Nematic topological semimetal and insulator in magic-angle bilayer graphene at charge neutrality, Phys. Rev. Research **3**, 013033 (2021).
[88] Yuan Da Liao, Zi Yang Meng, and Xiao Yan Xu, Valence Bond Orders at Charge Neutrality in a Possible Two-Orbital Extended Hubbard Model for Twisted Bilayer Graphene, Phys. Rev. Lett. **123**, 157601 (2019).
[89] Yuan Da Liao, Jian Kang, Clara N. Breiø, Xiao Yan Xu, Han-Qing Wu, Brian M. Andersen, Rafael M. Fernandes, and Zi Yang Meng, Correlation-Induced Insulating Topological Phases at Charge Neutrality in Twisted Bilayer Graphene, Phys. Rev. X **11**, 011014 (2021).
[90] Laura Classen, Carsten Honerkamp, and Michael M. Scherer, Competing phases of interacting electrons on triangular lattices in moiré heterostructures, Phys. Rev. B **99**, 195120 (2019).
[91] Dante M. Kennes, Johannes Lischner, and Christoph Karrasch, Strong correlations and $d + id$ superconductivity in twisted bilayer graphene, Phys. Rev. B **98**, 241407 (R) (2018).
[92] P. Myles Eugenio and Ceren B. Dağ, DMRG study of strongly interacting $\mathbb{Z}_2$ flatbands: A toy model inspired by twisted bilayer graphene, SciPost Phys. Core **3**, 15 (2020).
[93] Yixuan Huang, Pavan Hosur, and Hridis K. Pal, Quasi-flat-band physics in a two-leg ladder model and its relation to magic-angle twisted bilayer graphene, Phys. Rev. B **102**, 155429 (2020).
[94] Tongyun Huang, Lufeng Zhang, and Tianxing Ma, Antiferromagnetically ordered mott insulator and $d + id$ superconductivity in twisted bilayer graphene: A quantum Monte Carlo study, Sci. Bull. **64**, 310 (2019).
[95] Huaiming Guo, Xingchuan Zhu, Shiping Feng, and Richard T. Scalettar, Pairing symmetry of interacting fermions on a twisted bilayer graphene superlattice, Phys. Rev. B **97**, 235453 (2018).
[96] Patrick J. Ledwith, Grigory Tarnopolsky, Eslam Khalaf, and Ashvin Vishwanath, Fractional Chern insulator states in twisted bilayer graphene: An analytical approach, Phys. Rev. Research **2**, 023237 (2020).
[97] Cécile Repellin, Zhihuan Dong, Ya-Hui Zhang, and T. Senthil, Ferromagnetism in Narrow Bands of Moiré Superlattices, Phys. Rev. Lett. **124**, 187601 (2020).
[98] Ahmed Abouelkomsan, Zhao Liu, and Emil J. Bergholtz, Particle-Hole Duality, Emergent Fermi Liquids, and Fractional Chern Insulators in Moiré Flatbands, Phys. Rev. Lett. **124**, 106803 (2020).
[99] Cécile Repellin and T. Senthil, Chern bands of twisted bilayer graphene: Fractional Chern insulators and spin phase transition, Phys. Rev. Research **2**, 023238 (2020).
[100] Rafael M. Fernandes and Jörn W. F. Venderbos, Nematicity with a twist: Rotational symmetry breaking in a moiré superlattice, Sci. Adv. **6**, eaba8834 (2020).
[101] Justin H. Wilson, Yixing Fu, S. Das Sarma, and J. H. Pixley, Disorder in twisted bilayer graphene, Phys. Rev. Research **2**, 023325 (2020).
[102] Jie Wang, Yunqin Zheng, Andrew J. Millis, and Jennifer Cano, Chiral approximation to twisted bilayer graphene: Exact intravalley inversion symmetry, nodal structure, and implications for higher magic angles, Phys. Rev. Research **3**, 023155 (2021).
[103] B. Andrei Bernevig, Zhi-Da Song, Nicolas Regnault, and Biao Lian, Twisted bilayer graphene. I. Matrix elements,

approximations, perturbation theory, and a $k \cdot p$ two-band model, Phys. Rev. B **103**, 205411 (2021).
[104] Zhi-Da Song, Biao Lian, Nicolas Regnault, and B. Andrei Bernevig, Twisted bilayer graphene. II. Stable symmetry anomaly, Phys. Rev. B **103**, 205412 (2021).
[105] Fang Xie, Aditya Cowsik, Zhi-Da Song, Biao Lian, B. Andrei Bernevig, and Nicolas Regnault, Twisted bilayer graphene. VI. An exact diagonalization study at nonzero integer filling, Phys. Rev. B **103**, 205416 (2021).
[106] Xu Zhang, Gaopei Pan, Yi Zhang, Jian Kang, and Zi Yang Meng, Momentum space quantum Monte Carlo on twisted bilayer graphene, Chin. Phys. Lett. **38**, 077305 (2021).
[107] Peter Cha, Aavishkar A Patel, and Eun-Ah Kim, Strange Metals from Melting Correlated Insulators in Twisted Bilayer Graphene, Phys. Rev. Lett. **127**, 266601 (2021).
[108] Dmitry V. Chichinadze, Laura Classen, and Andrey V. Chubukov, Nematic superconductivity in twisted bilayer graphene, Phys. Rev. B **101**, 224513 (2020).
[109] Yarden Sheffer and Ady Stern, Chiral magic-angle twisted bilayer graphene in a magnetic field: Landau level correspondence, exact wave functions and fractional Chern insulators, Phys. Rev. B **104**, L121405 (2021).
[110] Jian Kang, B Andrei Bernevig, and Oskar Vafek, Cascades Between Light and Heavy Fermions in the Normal State of Magic Angle Twisted Bilayer Graphene, Phys. Rev. Lett. **127**, 266402 (2021).
[111] Johannes S Hofmann, Eslam Khalaf, Ashvin Vishwanath, Erez Berg, and Jong Yeon Lee, Fermionic Monte Carlo study of a realistic model of twisted bilayer graphene, arXiv:2105.12112.
[112] M. J. Calderón and E. Bascones, Interactions in the 8-orbital model for twisted bilayer graphene, Phys. Rev. B **102**, 155149 (2020).
[113] Alex Thomson and Jason Alicea, Recovery of massless Dirac fermions at charge neutrality in strongly interacting twisted bilayer graphene with disorder, Phys. Rev. B **103**, 125138 (2021).
[114] Ming Xie and A. H. MacDonald, Nature of the Correlated Insulator States in Twisted Bilayer Graphene, Phys. Rev. Lett. **124**, 097601 (2020).
[115] See Supplemental Material at http://link.aps.org/supplemental/10.1103/PhysRevLett.129.047601, for details of the contruction of the model and the Hartree-Fock calculation. It includes Refs. [1,2,4–7,10,21,25,36, 41,85,86,96,98,99,102,104,109,110,116–125].
[116] Nicola Marzari and David Vanderbilt, Maximally localized generalized Wannier functions for composite energy bands, Phys. Rev. B **56**, 12847 (1997).
[117] Ivo Souza, Nicola Marzari, and David Vanderbilt, Maximally localized Wannier functions for entangled energy bands, Phys. Rev. B **65**, 035109 (2001).
[118] Giovanni Pizzi *et al.*, Wannier90 as a community code: New features and applications, J. Phys. Condens. Matter **32**, 165902 (2020).
[119] Luis Elcoro, Benjamin J Wieder, Zhida Song, Yuanfeng Xu, Barry Bradlyn, and B Andrei Bernevig, Magnetic topological quantum chemistry, Nat. Commun. **12**, 5965 (2021).
[120] Yuanfeng Xu, Luis Elcoro, Zhi-Da Song, Benjamin J Wieder, MG Vergniory, Nicolas Regnault, Yulin Chen, Claudia Felser, and B. Andrei Bernevig, High-throughput calculations of magnetic topological materials, Nature (London) **586**, 702 (2020).
[121] Roland Winkler, *Spin-Orbit Coupling Effects in Two-Dimensional Electron and Hole Systems* (Springer Science & Business Media, Springer Berlin, Heidelberg, 2003).
[122] Dumitru Călugăru, Aaron Chew, Luis Elcoro, Nicolas Regnault, Zhi-Da Song, and B. Andrei Bernevig, General construction and topological classification of all magnetic and non-magnetic flat bands, Nat. Phys. **18**, 185 (2022).
[123] S. M. Girvin, A. H. MacDonald, and P. M. Platzman, Magneto-roton theory of collective excitations in the fractional quantum Hall effect, Phys. Rev. B **33**, 2481 (1986).
[124] Siddharth A. Parameswaran, Rahul Roy, and Shivaji L. Sondhi, Fractional quantum Hall physics in topological flat bands, C. R. Phys. **14**, 816 (2013).
[125] Rahul Roy, Band geometry of fractional topological insulators, Phys. Rev. B **90**, 165139 (2014).
[126] Barry Bradlyn, L. Elcoro, Jennifer Cano, M. G. Vergniory, Zhijun Wang, C. Felser, M. I. Aroyo, and B. Andrei Bernevig, Topological quantum chemistry, Nature (London) **547**, 298 (2017).
[127] Hoi Chun Po, Haruki Watanabe, and Ashvin Vishwanath, Fragile Topology and Wannier Obstructions, Phys. Rev. Lett. **121**, 126402 (2018).
[128] Junyeong Ahn, Sungjoon Park, and Bohm-Jung Yang, Failure of Nielsen-Ninomiya Theorem and Fragile Topology in Two-Dimensional Systems with Space-Time Inversion Symmetry: Application to Twisted Bilayer Graphene at Magic Angle, Phys. Rev. X **9**, 021013 (2019).
[129] Adrien Bouhon, Annica M. Black-Schaffer, and Robert-Jan Slager, Wilson loop approach to fragile topology of split elementary band representations and topological crystalline insulators with time-reversal symmetry, Phys. Rev. B **100**, 195135 (2019).
[130] Jennifer Cano, Barry Bradlyn, Zhijun Wang, L. Elcoro, M. G. Vergniory, C. Felser, M. I. Aroyo, and B. Andrei Bernevig, Topology of Disconnected Elementary Band Representations, Phys. Rev. Lett. **120**, 266401 (2018).
[131] Aline Ramires and Jose L. Lado, Emulating Heavy Fermions in Twisted Trilayer Graphene, Phys. Rev. Lett. **127**, 026401 (2021).
[132] Qimiao Si and Frank Steglich, Heavy fermions and quantum phase transitions, Science **329**, 1161 (2010).
[133] Philipp Gegenwart, Qimiao Si, and Frank Steglich, Quantum criticality in heavy-fermion metals, Nat. Phys. **4**, 186 (2008).
[134] Piers Coleman, New approach to the mixed-valence problem, Phys. Rev. B **29**, 3035 (1984).
[135] Maxim Dzero, Kai Sun, Victor Galitski, and Piers Coleman, Topological Kondo Insulators, Phys. Rev. Lett. **104**, 106408 (2010).
[136] A. M. Tsvelik and P. B. Wiegmann, Exact results in the theory of magnetic alloys, Adv. Phys. **32**, 453 (1983).
[137] Philipp Werner, Armin Comanac, Luca de' Medici, Matthias Troyer, and Andrew J. Millis, Continuous-Time

Solver for Quantum Impurity Models, Phys. Rev. Lett. **97**, 076405 (2006).

[138] Feng Lu, JianZhou Zhao, Hongming Weng, Zhong Fang, and Xi Dai, Correlated Topological Insulators with Mixed Valence, Phys. Rev. Lett. **110**, 096401 (2013).

[139] Hongming Weng, Jianzhou Zhao, Zhijun Wang, Zhong Fang, and Xi Dai, Topological Crystalline Kondo Insulator in Mixed Valence Ytterbium Borides, Phys. Rev. Lett. **112**, 016403 (2014).

[140] G. Kotliar, S. Y. Savrasov, K. Haule, V. S. Oudovenko, O. Parcollet, and C. A. Marianetti, Electronic structure calculations with dynamical mean-field theory, Rev. Mod. Phys. **78**, 865 (2006).

[141] V. J. Emery and S. Kivelson, Mapping of the two-channel Kondo problem to a resonant-level model, Phys. Rev. B **46**, 10812 (1992).

[142] Frederic Freyer, Jan Attig, SungBin Lee, Arun Paramekanti, Simon Trebst, and Yong Baek Kim, Two-stage multipolar ordering in PrT_2Al_{20} Kondo materials, Phys. Rev. B **97**, 115111 (2018).

[143] Akira Furusaki and Naoto Nagaosa, Kondo Effect in a Tomonaga-Luttinger Liquid, Phys. Rev. Lett. **72**, 892 (1994).

[144] Carlos R. Cassanello and Eduardo Fradkin, Kondo effect in flux phases, Phys. Rev. B **53**, 15079 (1996).

[145] Ivar Martin, Yi Wan, and Philip Phillips, Size Dependence in the Disordered Kondo Problem, Phys. Rev. Lett. **78**, 114 (1997).

[146] Sudip Chakravarty and Joseph Rudnick, Dissipative Dynamics of a Two-State System, the Kondo Problem, and the Inverse-Square Ising Model, Phys. Rev. Lett. **75**, 501 (1995).